Interdiffusion of CdS and Zn_2SnO_4 layers and its application in CdS/CdTe polycrystalline thin-film solar cells

X. Wu,[a] S. Asher, D. H. Levi, D. E. King, Y. Yan, T. A. Gessert, and P. Sheldon
National Renewable Energy Laboratory (NREL), 1617 Cole Boulevard, Golden, Colorado 80401

(Received 28 June 2000; accepted for publication 2 January 2001)

In this work, we found that the interdiffusion of the CdS and Zn_2SnO_4 (ZTO) layers can occur either at high temperature (550–650 °C) in Ar or at lower temperature (400–420 °C) in a $CdCl_2$ atmosphere. By integrating a Zn_2SnO_4 film into a CdS/CdTe solar cell as a buffer layer, this interdiffusion feature can solve several critical issues and improve device performance and reproducibility of both SnO_2-based and Cd_2SnO_4-based CdTe cells. Interdiffusion consumes the CdS film from both the ZTO and CdTe sides during the device fabrication process and improves quantum efficiency at short wavelengths. The ZTO film acts as a Zn source to alloy with the CdS film, which results in increases in the band gap of the window layer and in short-circuit current density J_{sc}. Interdiffusion can also significantly improve device adhesion after $CdCl_2$ treatment, thus providing much greater process latitude when optimizing the $CdCl_2$ process step. The optimum $CdCl_2$-treated CdTe device has high quantum efficiency at long wavelength, because of its good junction properties and well-passivated CdTe film. We have fabricated a Cd_2SnO_4/Zn_2SnO_4/CdS/CdTe cell demonstrating an NREL-confirmed total-area efficiency of 15.8% (V_{oc} = 844.3 mV, J_{sc} = 25.00 mA/cm^2, and fill factor = 74.82%). This high-performance cell is one of the best thin-film CdTe solar cells in the world. © *2001 American Institute of Physics.*
[DOI: 10.1063/1.1351539]

I. INTRODUCTION

CdTe is a promising photovoltaic material for thin-film solar cells because of its near optimum band gap (~1.5 eV) and its high absorption coefficient. Lab-scale CdTe cells with 15.8% efficiencies have been demonstrated. However, performance and reproducibility of CdTe thin-film solar cells have been limited by several critical issues that relate to the conventional SnO_2/CdS/CdTe device structure. One of these issues is that conventional SnO_2 transparent conductive oxide (TCO) films have an inherent sheet resistivity of ~10 Ω/sq and an average transmission of 80%. This does not provide adequate design latitude when trying to optimize device performance. Indium–tin–oxide films (~90% In_2O_3, ~10% SnO_2) have excellent electrical and optical properties, and were used as the transparent front-contact layer in CdTe cells.[1–3] But its application in photovoltaic devices has been limited by its cost. In recent years, we have performed extensive research on improved TCOs, including cadmium stannate (Cd_2SnO_4, or CTO) and zinc stannate (Zn_2SnO_4, or ZTO) films. We found that cadmium stannate TCO films have several advantages over SnO_2 TCO films.[4–6] They have resistivities ($\rho = 1.5\times10^{-4}$ Ω cm) 2–6 times lower than SnO_2 films and have an average surface roughness (R_a~20 Å) an order of magnitude lower than SnO_2 films produced using a $SnCl_4$ chemistry. CTO films have been produced with a sheet resistance of ~10 Ω/sq and a peak transmission of near 90% at 500 nm. In a CdTe cell, replacing the SnO_2 layer with CTO can improve the device's short-circuit current density J_{sc} and fill factor (FF). CTO-based CdTe cells have an average J_{sc} that is 1 mA/cm^2 higher than SnO_2-based cells. But, there are other issues that limit device performance and reproducibility in conventional CdTe devices. For example, higher J_{sc} can be achieved by reducing CdS thickness to improve a device's blue spectral response. However, reducing the CdS thickness can adversely impact the open-circuit voltage V_{oc} and FF of CdTe cells.[7] In addition, it is well known that the $CdCl_2$ treatment is important for making high-efficiency CdTe devices and offers several substantial benefits. However, one disadvantage of the $CdCl_2$ treatment is that overtreatment can result in loss of adhesion. The adhesion problems can limit the optimal $CdCl_2$ treatment process, as well as device performance.[8]

Our earlier work identified several key features regarding the interaction between the CdS and ZTO layers:[9,10] (1) recrystallization of zinc stannate films deposited at room temperature in pure oxygen can be enhanced when annealed in a CdS/Ar atmosphere; and (2) optical and electrical properties of the ZTO film annealed in a CdS/Ar atmosphere are better than for films annealed in pure Ar. We do not completely understand how CdS enhances the recrystallization and performance of ZTO film, but we have evidence of a chemical reaction between the CdS and ZTO layers. We can expect that by integrating a ZTO layer into a CdS/CdTe solar cell, this feature can improve the TCO/CdS interface, thus improving device performance.

The purpose of this work is to: (1) further study the chemical reaction between the CdS and ZTO layers; and (2) try to exploit this chemical reaction to solve some critical issues by integrating a ZTO film into CdTe devices as a

[a]Electronic mail: xuanzhi_wu@nrel.gov

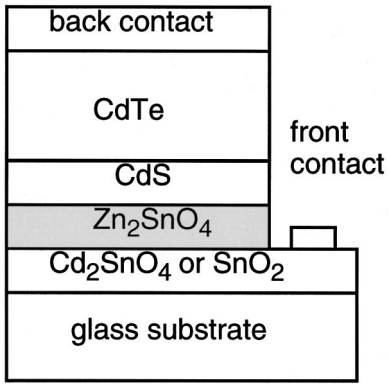

FIG. 1. A modified CdS/CdTe device structure used in this study.

buffer layer between the CdS and TCO layers.

II. EXPERIMENT

A series of CdTe cells, with a modified device structure shown in Fig. 1, was prepared for demonstrating the application of interdiffusion of the CdS and ZTO layers. In this modified device structure, the Zn_2SnO_4 layer is integrated into the device as a buffer layer. In this study, most cells were fabricated on CTO-based superstrates. But, a limited number of cells were prepared on SnO_2–TCO films to demonstrate the usefulness of a ZTO buffer layer not only for CTO-based superstrates, but also, for SnO_2-based devices. For comparison, a number of cells with CTO/CdS/CdTe or SnO_2/CdS/CdTe device structure have also been produced. The thickness of CTO and ZTO layers was varied from 100 to 300 nm. The CdS layer was deposited by a chemical-bath deposition (CBD) technique,[11] using cadmium acetate $[Cd(C_2H_3O_2)_2]$, ammonium acetate $(NH_4C_2H_3O_2)$, ammonia hydroxide (NH_4OH), and thiourea $(CS(NH_2)_2)$ in an aqueous solution. The CdTe films were prepared by the close-spaced sublimation (CSS) technique and were deposited at 570–625 °C for 3–5 min. After CSS deposition of the CdTe, the substrates were treated in $CdCl_2$ vapor at 400–420 °C for 15 min. CuTe:HgTe-doped graphite paste, followed by a layer of Ag paste, was then applied to the devices as the back-contact layer.

The devices were characterized by measuring their standard current density/voltage performance in the light and dark. We thus obtained J_{sc}, V_{oc}, FF, saturation dark current density J_0, and diode factor A. We also measured the absolute external and internal quantum efficiencies of the devices, as well as time-resolved photoluminescence lifetimes.

III. INTERDIFFUSION OF THE CdS AND ZTO LAYERS

X-ray photoemission spectroscopy (XPS) and secondary-ion mass spectroscopy (SIMS) results have shown that interdiffusion of the CdS and ZTO layers can occur either at high temperature (550–650 °C) in Ar or at lower temperature (400–420 °C) in a $CdCl_2$ atmosphere. To study interdiffusion at the CdS/ZTO interface, special samples were prepared as follows: (1) Sample preparation for XPS measurement. The Zn_2SnO_4 films were deposited on 7059 Corning glass substrates by rf magnetron sputtering. A commercial hot-pressed-oxide target with a composition of 33 mol % SnO_2 and 67 mol % ZnO was used. Deposition was performed in pure oxygen at room temperature, as previously described.[9,10] The CdS films were prepared on 7059 Corning glass substrates by the CBD technique. After deposition, two ZTO films were placed face down on CdS films and annealed in flowing pure Ar at temperatures of 600 and 650 °C, respectively. XPS was used to measure the composition changes of both the CdS and the ZTO film before and after annealing. (2) Sample preparation for SIMS and transmission electron microscopy (TEM) measurements. The CdS film and the ZTO film were deposited sequentially on a 7059 Corning glass or on a Si wafer with a pure SiO_2 film, which prevents impurities from diffusing from Si to the CdS and ZTO layers. These samples were annealed in a $CdCl_2$ atmosphere at 400–420 °C.

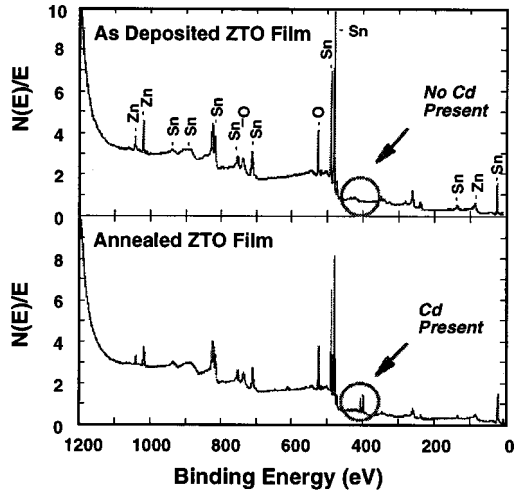

(a) ZTO film

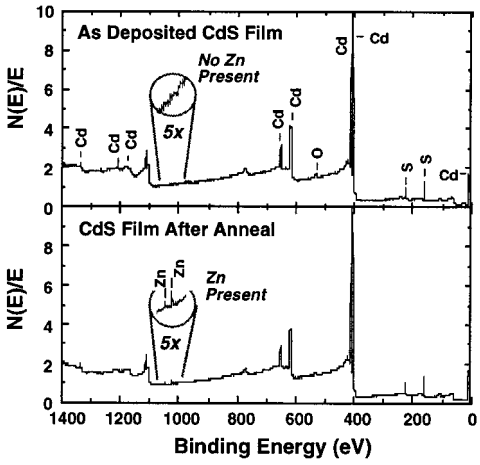

(b) CdS film

FIG. 2. XPS survey spectra of the ZTO film (a) and the CdS film (b) before and after annealing.

TABLE I. The deduced atomic concentrations of the ZTO and CdS films before and after annealing at ~600 °C for 5 min.

Sample No.	Position	Sn (at. %)	Zn (at. %)	O (at. %)	Cd (at. %)	S (at. %)
ZTO Before annealing	Surface	30.6	13.0	56.1	0.1	0.3
	300 Å depth	26.1	22.8	51.2	0.0	0.0
ZTO After annealing	Surface	32.2	9.1	55.1	2.8	0.7
	300 Å depth	24.8	21.5	50.5	3.2	0.0
CdS Before annealing	Surface	0.0	0.0	10.1	51.8	38.1
	300 Å depth	0.0	0.0	11.9	51.5	36.6
CdS After annealing	Surface	0.0	2.3	11.3	48.2	38.3
	300 Å depth	0.0	2.1	11.2	48.4	38.3

A. Interdiffusion at high temperature

Figure 2 shows XPS survey spectra of the ZTO film and the CdS film before and after face-to-face annealing. Figure 2(a) indicates the absence of Cd in the ZTO film before annealing within the detection limits of XPS, and about 4.3 at. % Cd diffuses into the ZTO film from the CdS layer after annealing at ~650 °C. Similarly, we do not see any Zn in the CdS film before annealing [Fig. 2(b)], and we can see about 2.4 at. % Zn in the CdS film after annealing at ~650 °C. Table I summarizes the atomic concentrations for the ZTO and CdS films before and after annealing at ~600 °C for 5 min. To ensure that the Cd and Zn were not just surface contamination, XPS measurements were taken at two different depths: at the surface and after the removal of ~300 Å of material. This result demonstrates that Cd and Zn are not limited to the surface, but actually diffuse a substantial distance into the ZTO and the CdS film, respectively.

B. Interdiffusion at lower temperatures (400–420 °C) in a $CdCl_2$ atmosphere

SIMS depth profiling was used to determine the extent of interdiffusion at the ZTO/CdS interface. Figure 3(a) shows the profile before annealing, and Fig. 3(b) shows the profile after annealing at 420 °C in a $CdCl_2$ atmosphere. A considerable amount of diffusion is observed in the annealed films. Additional experiments showed that interdiffusion was minimal at the ZTO and CdS interface when the sample was annealed in Ar at the same temperature and length of time. This result demonstrates that the $CdCl_2$ treatment enhances the extent of interdiffusion between the ZTO and CdS films.

Figure 4 shows cross-sectional TEM images of a ZTO/CdS/SiO_2/*c*-Si sample annealed at 420 °C in a $CdCl_2$ atmosphere for 15 min. For clarity, the SiO_2 and *c*-Si layers are not shown in the figure. Figure 4(a) shows the microstructure of the film at the interface region, whereas Fig. 4(b) shows a ZTO region far away from the interface. The position of the interface is marked by a white dashed line in Fig. 4(a). We found that the CBD-grown CdS layer is fully crystallized. In the ZTO layer, the regions near the surface are crystallized, as seen in Fig. 4(b). However, such crystallization is not clearly observed in the samples annealed in pure Ar at the same temperature. We thus believe that a $CdCl_2$ atmosphere enhances the crystallization of the ZTO film, which helps to improve its optical and electrical properties. We also found that the ZTO regions near the interface still remain amorphous, as seen in Fig. 4(a). We suspect that the remaining amorphous ZTO near the interface is caused by interdiffusion between the CdS and ZTO layers.

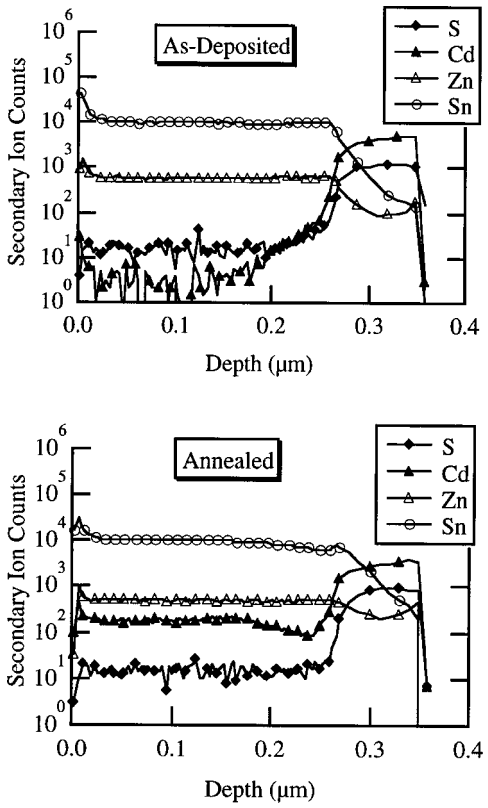

FIG. 3. SIMS data showing the interdiffusion of the ZTO and CdS films at 420 °C in $CdCl_2$ atmosphere.

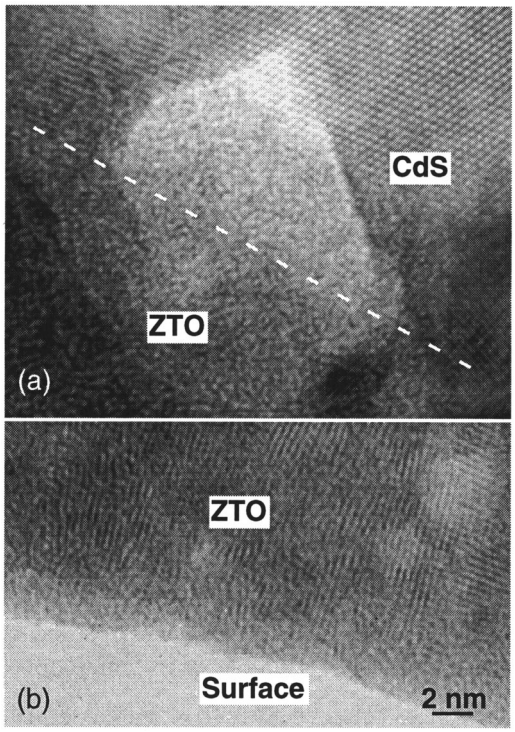

FIG. 4. TEM image of a ZTO/CdS/SiO_2/*c*-Si sample annealed at 420 °C in $CdCl_2$ atmosphere: (a) at interface; (b) ZTO region far from interface.

IV. APPLICATION OF THE INTERDIFFUSION OF ZTO AND CdS FILMS IN CdTe SOLAR CELLS

We have integrated a ZTO film into CdS/CdTe devices as a buffer layer (see Fig. 1) and have successfully applied the interdiffusion feature to solve several critical issues and improve the device performance and reproducibility. Table II lists the current–voltage ($I-V$) data of the four best CdTe cells with different device structures. We can see that the efficiencies of both CTO-based and SnO_2-based cells with a ZTO buffer layer have been significantly improved. We have fabricated a Cd_2SnO_4/Zn_2SnO_4/CdS/CdTe cell demonstrating an NREL-confirmed total-area ($0.647\,cm^2$) efficiency of 15.8% ($V_{oc}=844.3\,mV$, $J_{sc}=25.00\,mA/cm^2$, and FF $=74.82\%$). This high-performance cell is one of the best CdTe cells in the world.[12,13] Figure 5 shows the relative external quantum efficiency (QE) of two cells with CTO/ZTO/CdS/CdTe and CTO/CdS/CdTe device structure, respectively. From this graph, we can demonstrate that interdiffusion of the ZTO and CdS layers improves the quantum efficiency of a CdTe cell over the entire active wavelength region (400–860 nm).

TABLE II. $I-V$ data of four best CdTe cells with different device structures.

Device structure	V_{oc} (mV)	J_{sc} (mA/cm^2)	FF (%)	η (%)
SnO_2/CdS/CdTe	806.7	22.61	74.02	13.5
CTO/CdS/CdTe	805.2	23.53	73.77	14.0
SnO_2/ZTO/CdS/CdTe	830.1	24.10	74.15	14.8
CTO/ZTO/CdS/CdTe	844.3	25.00	74.82	15.8

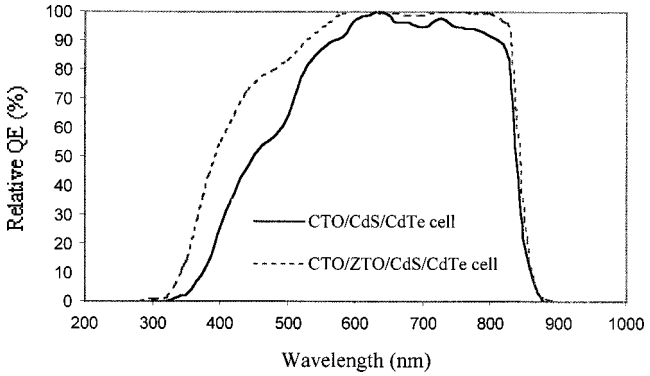

FIG. 5. Relative quantum efficiency of two CdTe cells with CTO/CdS/CdTe and CTO/ZTO/CdS/CdTe device structure, respectively.

(1) Interdiffusion occurs at both the CdS/ZTO and the CdS/CdTe interface, thereby consuming the CdS layer and improving the quantum efficiency in the short-wavelength region of 400–510 nm. It is well known that higher short-circuit currents can be obtained by reducing the window-layer absorption in heterojunction solar cells. In CdS/CdTe cells, this is achieved by reducing the CdS thickness. However, by reducing the CdS layer thickness too much, one can adversely impact the device open-circuit voltage V_{oc} and FF. As the CdS layer is thinned, the probability of pinhole formation in CdS film increases. Fourier transform infrared measurement results demonstrated that the pinhole density in a ~500 Å CBD CdS film is 2–4 times higher than that in a 1000 Å CBD CdS film. The pinholes in CdS film cause localized TCO/CdTe junctions with inferior device performance (V_{oc} and FF). Although some researchers have produced high-efficiency devices by minimizing the thickness of the CdS window layer (50–65 nm), the performance of these has typically been somewhat irreproducible. Absolute QEs at 450 nm in these high-efficiency CdTe cells were 50%–60%. To maintain higher yields, most CdTe module manufacturers must use a thicker CdS film in their fabrication process, yielding CdTe modules with very low J_{sc} ($18-20\,mA/cm^2$). The typical absolute external QEs of the CdTe modules at 450 nm were only 10%–25%. In our modified device structure, the CdS film has a thickness of ~80 nm, with a lower pinhole density. We can see from Fig. 5 that the modified CTO/ZTO/CdS/CdTe cell with a thicker CdS film (~800 Å) has an absolute external QE of ~70% at 450 nm, which is substantially greater than conventional cells with thinner CdS layers. From Fig. 5, we can also see that QE of a CTO/ZTO/CdS/CdTe cell is much better than that of a CTO/CdS/CdTe cell at the short-wavelength region. These results indicate that a considerable amount of CdS can be consumed through interdiffusion at both the CdTe and the ZTO sides during the device fabrication process. This property may be exploited in production by using thicker CdS films, thereby enhancing reproducibility, without reducing J_{sc}.

(2) In the interdiffusion of the CdS and ZTO films, the ZTO film acts as a Zn source to alloy with the CdS film. From the literature,[14] the bowing parameter in the CdS/ZnS system is small, and the band gap of $Zn_xCd_{1-x}S$ varies almost

TABLE III. Significantly improved adhesion after $CdCl_2$ treatment.

	CdTe cells without ZTO layer	SnO_2-based cells with ZTO layer	CTO-based cells with ZTO layer
Total number of devices	14	21	63
Good adhesion	1 (7%)	19 (90%)	60 (95%)
Blister on edges	8 (57%)	2 (10%)	3 (5%)
Completely peeled off	5 (36%)	0 (0%)	0 (0%)

linearly with the atomic fraction of zinc (x). The band gap of CdS is reported as 2.4 eV, whereas that of ZnS is 3.8 eV. Consequently, as Zn from zinc stannate diffuses into and alloys with the CdS film, the band gap increases. This shifts the short-wavelength cutoff to a smaller value, which leads to an increase in J_{sc}. Cd diffusing from CdS film into the ZTO film can help to reduce resistivity of the ZTO layer. Because ZTO film was deposited in pure O_2 at room temperature by rf sputtering, an as-grown ZTO film has an amorphous microstructure and a very high resistivity ($\sim 10^4\,\Omega$ cm). After CdTe layer deposition (typically at 550–630 °C), the ZTO film changed to a polycrystalline spinel structure and its resistivity was reduced to 1–10 Ω cm, which roughly matches that of CdS film.

(3) An additional advantage is that interdiffusion between the CdS and ZTO layers can significantly improve film adhesion after $CdCl_2$ treatment. Performance and reproducibility of CdTe cells are significantly influenced by the $CdCl_2$ treatment, which is used by all cell manufacturers. The $CdCl_2$ treatment is an important process for making high-efficiency CdTe devices and offers several substantial benefits such as: increased grain size, grain-boundary passivation, increased CdS/CdTe interface alloying, and reduced lattice mismatch between the CdS and CdTe films. However, one disadvantage of the $CdCl_2$ treatment is that overtreatment can result in adhesion-loss problems. Grain growth of the CdS film, which occurs during the $CdCl_2$ treatment, may introduce stress at the interface between the CdS and SnO_2–TCO layers, resulting in film blistering or peeling.

The interdiffusion between the CdS and ZTO layers may relieve the stress at the CdS/ZTO interface, thereby improving device adhesion. Table III shows that integrating the ZTO buffer layer into CdTe cells can significantly improve the adhesion after $CdCl_2$ treatment. A total of 98 CdTe devices, each of which received a 100%-saturated $CdCl_2$ solution soak (50%–75% $CdCl_2$ solution is typical) and subsequent thermal anneal, were fabricated for evaluation of device adhesion. Eighty-four of these devices, including 21 SnO_2-based and 63 CTO-based cells, had the ZTO buffer layer integrated into the device structure, and 14 did not. Without the buffer layer, under these extreme conditions, we found that only one cell had good adhesion out of a total of 14 cells (7% yield). In sharp contrast with the ZTO buffer layer, 19 SnO_2-based cells and 60 CTO-based cells had good adhesion out of 21 cells (90% yield) and 63 cells (95% yield), respectively. This result has significant ramifications for manufacturing: the ZTO buffer layer provides far better adhesion, leading to high yield.

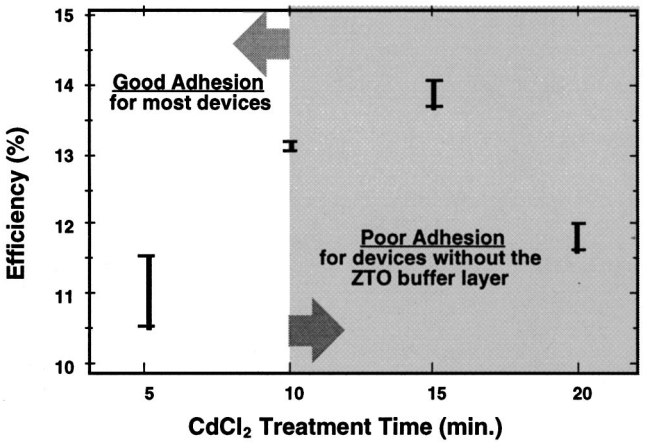

FIG. 6. Correlation of ZTO buffer-layer integrated CdTe cell efficiencies and vapor $CdCl_2$ treatment time (treatment temperature fixed at 400 °C).

(4) The improvement of device adhesion provides much greater latitude in optimizing the $CdCl_2$ treatment process, leading to improved device junction properties and CdTe film quality. Figure 6 shows the correlation between CdTe cell efficiencies (that include a ZTO buffer layer) and vapor $CdCl_2$ treatment time. The $CdCl_2$ temperature was fixed at 400 °C. We can see that CdTe cells without the ZTO buffer layers have adhesion problems before the optimum $CdCl_2$ treatment conditions are reached.

Time-resolved photoluminescence (TRPL) was measured at room temperature under open-circuit conditions. Photoexcitation is through the transparent CdS window layer at a wavelength of 600 nm. Average laser power is 10 mW at a 1 MHz repetition rate with a 1-mm-diam spot. This generates an initial photoexcited carrier density of about $2\times10^{16}\,\mathrm{cm}^{-3}$. The $1/e$ penetration depth for 600 nm light in CdTe is 0.2 μm. Numerical modeling indicates that more than 90% of the photoexcited carriers recombine within 1 μm of the CdTe/CdS interface. Thus, this technique probes the quality of the CdTe material nearest the junction, and it is referred to as ''junction photoluminescence.'' Polycrystalline materials, such as the CdTe layer in CdTe/CdS solar cells, contain high concentrations of traps. It is difficult to separate out the effects of capture and emission of carriers in traps from recombination processes. Hence, TRPL in these

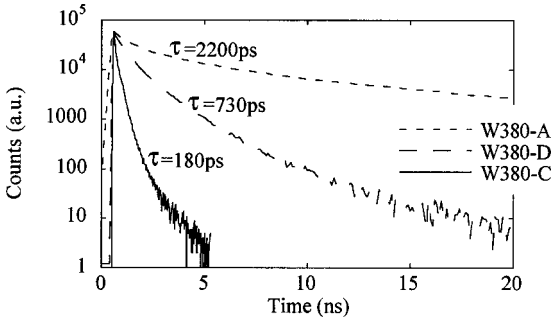

FIG. 7. TRPL decay curves of three CdTe cells with different $CdCl_2$ treatments.

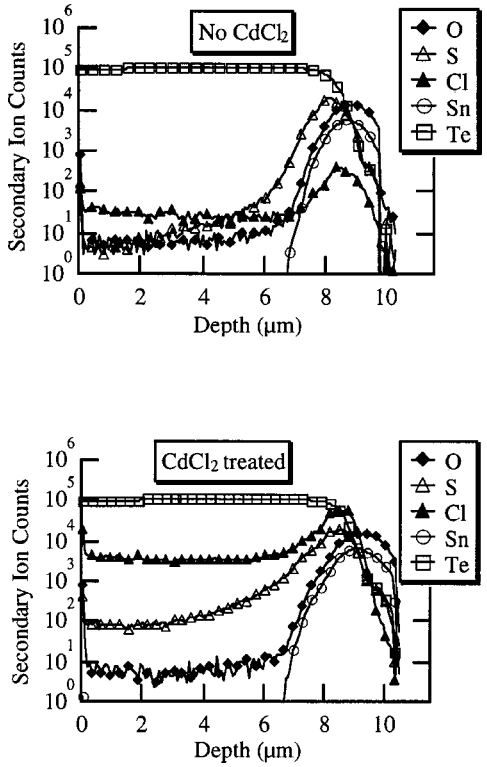

FIG. 8. SIMS profiles show the change in a CTO/ZTO/CdS/CdTe cell after $CdCl_2$ treatment.

materials is a good indicator of the minority-carrier lifetime, but is not equal to the minority-carrier lifetime. The results of junction TRPL measurements on three samples are shown in Fig. 7. The optimum $CdCl_2$-treated device (W380-A) has a TRPL lifetime that is three times longer than that of the conventional $CdCl_2$-treated device (W380-D). The device without a $CdCl_2$ treatment (W380-C) has the shortest lifetime at 180 ps. The CdTe cell with the longest lifetime has the best junction properties and a well-passivated CdTe film. This is confirmed by measurements of saturated dark current density J_0 and diode factor A. The J_0 and A of the optimum $CdCl_2$-treated cell are $7.5\times10^{-11}\,A/cm^2$ and 1.62, respectively. In contrast, the J_0 and A of the conventional $CdCl_2$-treated cell are $8.2\times10^{-9}\,A/cm^2$ and 1.90, respectively.

Figure 8 shows SIMS depth profiles from two of the devices discussed above: Figure 8(a) shows the device with no $CdCl_2$ treatment, and Fig. 8(b) shows the device with optimal $CdCl_2$ treatment. The profile shows that a considerable amount of S and Cl diffusion has occurred during the $CdCl_2$ treatment. The higher level of S and Cl in the CdTe bulk of the optimal $CdCl_2$-processed device helps to passivate the CdTe layer. This is consistent with the longer TRPL lifetime for this device.

We can see that in Fig. 5, the optimum $CdCl_2$-treated CTO/ZTO/CdS/CdTe cell has nearly 100% absolute internal QE in the long-wavelength region of 580–840 nm. In contrast, the CTO/CdS/CdTe cell with normal $CdCl_2$ treatment has much poorer QE at the long-wavelength region. All measurement results described in this section can explain this fact, because of the former cell's excellent junction properties and its well-passivated CdTe film.

V. CONCLUSION

The interdiffusion of the CdS and ZTO layers can occur either at high temperature (550–650 °C) in Ar or at lower temperature (400–420 °C) when annealed in a $CdCl_2$ atmosphere. This interdiffusion can improve device performance and reproducibility of both CTO-based and SnO_2-based CdTe cells. Interdiffusion consumes the CdS film from both the ZTO and CdTe sides during the device fabrication process and improves quantum efficiency at short wavelengths. The ZTO film acts as a Zn source to alloy with the CdS film, which results in an increase in the band gap of the window layer and in J_{sc}. Interdiffusion can also significantly improve device adhesion after $CdCl_2$ treatment, thus providing much greater process latitude when optimizing the $CdCl_2$ process step. The optimum $CdCl_2$-treated CdTe device has high quantum efficiency at long wavelength because of its good junction properties and well-passivated CdTe film. Finally, we have developed a reliable fabrication procedure that enabled us to achieve a $Cd_2SnO_4/Zn_2SnO_4/CdS/CdTe$ cell demonstrating an NREL-confirmed total-area efficiency of 15.8% ($V_{oc}=844.3\,mV$, $J_{sc}=25.00\,mA/cm^2$, and FF $=74.82\%$). This high-performance cell is one of the best CdTe thin-film solar cells in the world.

ACKNOWLEDGMENTS

The authors would like to thank K. Emery, T. Moriarty, and D. Dunlavy for the measurements of standard $I-V$ and QE measurements, and R. Ribelin for CBD CdS deposition. This work is supported by the U.S. Department of Energy under Contract No. DE-AC36-99GO10337 to the National Renewable Energy Laboratory.

[1] D. Bonnet and M. Harr, Proceedings of the 2nd World Conference and Exhibition on PVSEC, 1998, pp. 397–402.
[2] N. Romeo, A. Bosio, R. Tedeschi, and V. Canevari, Proceedings of the 2nd World Conference and Exhibition on PVSEC, 1998, pp. 446–447.
[3] B. E. McCandless, National CdTe R&D Meeting Minutes, 1999.
[4] X. Wu, P. Sheldon, T. J. Coutts, D. H. Rose, W. P. Mulligan, and H. R. Moutinho, Proceedings of the 14th NREL/SNL PV Program Review Meeting, 1996, pp. 693–702.
[5] X. Wu, P. Sheldon, T. J. Coutts, D. H. Rose, and H. R. Moutinho, Proceedings of the 26th IEEE PVSC, 1997, pp. 347–350.
[6] X. Wu, T. J. Coutts, P. Sheldon, and D. H. Rose, U.S. Patent No. 5922142 (1999).
[7] B. E. McCandless and S. S. Hegedus, Proceedings of the 22nd IEEE PVSC, 1991, pp. 967–972.
[8] X. Wu, P. Sheldon, Y. Mahathongdy, R. Ribelin, A. Mason, H. R. Moutinho, and T. J. Coutts, Proceedings of the 15th NREL/SNL PV Program Review Meeting, 1998, pp. 37–41.
[9] X. Wu, W. P. Mulligan, and T. J. Coutts, Proceedings Society of Vacuum Coaters, Philadelphia, PA, 1996, p. 217.
[10] X. Wu, T. J. Coutts, and W. P. Mulligan, J. Vac. Sci. Technol. A **15**, 1057 (1997).
[11] T. L. Chu, S. S. Chu, N. Schultz, C. Wang, and C. Q. Wu, J. Electrochem. Soc. **139**, 2443 (1992).
[12] J. Britt and C. Ferekides, Appl. Phys. Lett. **62**, 2851 (1993).
[13] H. Ohyama *et al.*, Proceedings 26th IEEE PVSC, 1997, pp. 343–346.
[14] H. Hartmann *et al.*, *Wide-Gap II-VI Compounds as Electronic Materials*, edited by E. Kaldis, Vol. 9, p. 58.